

Remote sensing to monitor changes over time: 2023 Emilia-Romagna flood

Benedetta Bensi

Artificial Intelligence for Science and Technology

Università degli Studi di Milano-Bicocca

867143

Email: b.bensi@campus.unimib.it

Abstract—Sentinel-2 provides high-resolution, multi-spectral imaging. For this reason it is widely employed in land and maritime monitoring, as well as emergency management. This report explores the application of Sentinel-2 for flood damage assessment which, combined with change detection techniques and machine learning, can be a powerful tool in taking crucial decisions after the disaster and supporting the assessment of the damages of the affected areas.

1. Introduction

The frequency and severity of natural disasters threatens human health as well as infrastructures and environment, making it crucial to find instruments able to give rapid and accurate damage assessment reports. In the last years, remote sensing technology proved its efficiency and comprehensiveness in disaster monitoring.

Emilia-Romagna, one of Italy's most important agricultural and industrial regions, has been hit by two severe flooding events within two weeks, starting from the first inundation occurred on 2nd May 2023. Between 16-18 May 2023, 350 million cubic metres of water, equivalent to six months' worth of rain, fell within 36 hours across Emilia-Romagna. The heavy rain led to the overflow of 23 rivers across the region, affecting 100 municipalities and triggering more than 400 landslides, in particular in the southern-eastern area of the region. More specifically, among the others, the breaking of the Sillaro River embankment and the overflow of the Lamone River produced flooding close to the cities of Massa Lombarda and Conselice. The emergency has been declared at national level and all components of the Italian Civil Protection System have been activated.

The support of satellites was though extremely crucial as they provided the ability to assess potential impacts of the natural disaster, assisted in emergency management activities and they could also support post-event analysis and damage assessment.

During this report Sentinel-2's 13 spectral bands are exploited so that, by combining them in various ways, it is possible to enhance the detection of specific features and changes in the landscape, making multi-spectral analysis a powerful tool for flood mapping. In addition to this, change

detection techniques are explored, in order to study and monitor land coverage before and after flood. Machine learning algorithms are employed too, particularly unsupervised methods like clustering, that can automate the analysis of satellites data, making the identification of flood-affected areas and the classification of land cover changes more efficient. Moreover, machine learning techniques can be combined with change detection methods, such as band differencing, to enhance the accuracy of flood mapping. In this way it is possible to refine the identification of flood-affected regions and distinguish between temporary water bodies and persistent changes in the landscape. The advantage in using machine learning in flood damage assessment is that not only it automates the analysis of the images, but also improves the precision and reliability of the results.

2. Data and methodology

2.1. Sentinel-2 overview

Sentinel-2 is an Earth observation mission from the European Space Agency's (ESA) Copernicus program, that provides continuous, high-quality Earth observation data for environmental monitoring and disaster management. Launched in June 2015, Sentinel-2 consists of a constellation of two identical satellites, Sentinel-2A and Sentinel-2B, in the same orbit but phased at 180°, which give a high revisit frequency of 5 days at the Equator.

The strength of Sentinel-2 resides in its Multi-Spectral Instrument (MSI), which captures data across 13 spectral bands, ranging from the visible spectrum to near-infrared (NIR) and short wave infrared (SWIR)¹. The spatial resolution of Sentinel-2's bands varies between 10, 20 and 60 meters:

- 4 x 10 metre bands: the three classical RGB bands and a Near Infra-Red band;
- 6 x 20 metre bands: 4 narrow Bands in the VNIR vegetation red edge spectral domain and 2 wider

1. For a better understanding and clarification consider to inspect table 1 in the Appendix section.

- SWIR bands for applications such as snow/ice/cloud detection, or vegetation moisture stress assessment;
- 3 x 60 metre bands mainly focused towards cloud screening and atmospheric correction and cirrus detection.

This high resolution allows for accurate mapping and analysis of specific areas, making it extremely useful in disaster scenarios, where precise data is crucial for assessing the extent of damage and planning recovery efforts. In the context of flood monitoring and damage assessment, Sentinel-2's multi-spectral data allows for the detection of water bodies, the assessment of vegetation health, and the identification of land cover changes before and after flood events. By utilizing various combinations of its spectral bands, change detection analyses can be performed, and the application of machine learning algorithms can automate the identification of flood-affected areas.

2.2. Preprocessing

The study focused on Emilia-Romagna region: a specific geographic location was selected (with coordinates latitude 44.696379, longitude 12.180427) as the reference point to define the area of interest. This point is used as the center of a circular region (a buffer with a radius of 45 kilometers); in this way the analysis covers both urban and rural regions affected by the flood.

To capture the land and maritime changes due to the flood, images were filtered to include only those taken between February 1, 2023, and April 30, 2023. This time frame was chosen to represent the pre-flood environment and establish a baseline for comparison with post-flood imagery. This interval of time was intentionally chosen this wide to provide a larger number of images also considering the cloud factor. As it regards the post-flood environment, since the flood occurred between 2-3 and 16-18 of May, images were filtered to comprehend only those taken between May 15, 2023 and May 25, 2023, in order to capture all the environmental consequences and patterns due to this natural disaster.

To ensure the quality of the data, the image collection was furtherly filtered to exclude images with more than 10% cloud cover. This threshold was set to minimize the impact of clouds on the analysis, in order to provide clear and accurate data for the following study. After filtering the image collection, the selected images were processed to create a single composite image that represents the median value of each pixel across all images in the collection.

To first inspect the data, I selected the red (B4), green (B3), and blue (B2) bands, which correspond to the visible spectrum. By combining these bands a true-color image is created, resembling what the human eye would see.

In Figures 1 and 2, the differences between the pre-flood and post-flood conditions are clearly visible. In the pre-flood image (Figure 1), the rivers and sea exhibit a typical blue colour, indicating clear water with minimal sediment. The land areas show no significant signs of water

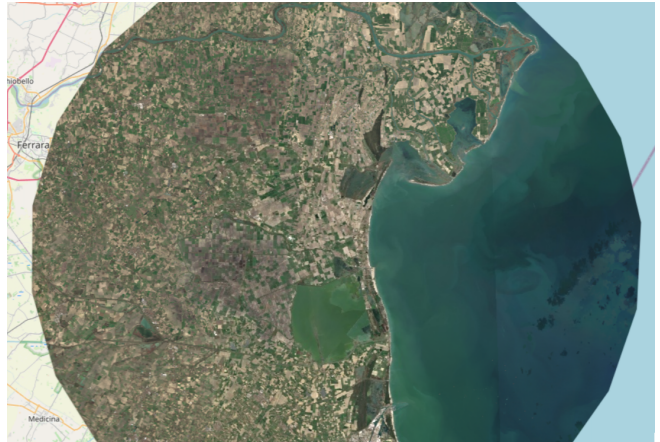


Figure 1. Region of interest before flood: B4, B3, B2 combined.

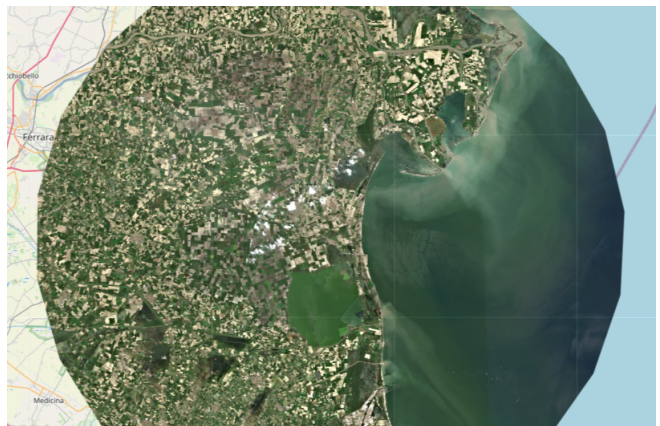


Figure 2. Region of interest after the flood: B4, B3, B2 combined.

invasion. On the contrary, the post-flood image (Figure 2) reveals significant changes: several regions reveal the sign of floodwaters. The colour of the rivers and the sea has changed to a more turbid brownish one, which is indicative of the presence of sediment and mud carried by the floodwaters. To better envision the presence of floodwaters in the region of interest and to apply in a more strategic way the change detection techniques, specific Sentinel-2 spectral bands can be exploited to enhance water bodies. By selecting bands B11 (Shortwave Infrared), B8 (Near-Infrared), and B3 (Green), water and other land cover types can be better distinguished. In fact water strongly absorbs light in the Near-Infrared (NIR) and Shortwave Infrared (SWIR) regions of the spectrum, making it appear very dark in these bands. Conversely, vegetation and soil reflect more light in B8 and B11 wavelengths, providing a clear contrast against water bodies. The inclusion of the Green band (B3) further enhances the ability to differentiate water from vegetation.

In figures 3 and 4 water bodies are now highlighted, floodwater is more visible and the impact of the disaster becomes more tangible. It is now clear that the flooded areas are near Conselice and Massa Lombarda, caused by



Figure 3. Region of interest before the flood: B11, B8, B3 combined.



Figure 4. Region of interest after the flood: B11, B8, B3 combined.

the breaking of Sillaro and Lamone river. This enhanced visibility not only aids in immediate disaster response but also contributes to a better understanding of the disaster's full scope.

The Normalized Difference Water Index (NDWI) particularly fits in the context of flood events since it is able to detect and monitor water bodies. NDWI is calculated using the Near-Infrared (NIR) and Green bands of Sentinel-2 imagery, and it is defined by the following formula:

$$NDWI = \frac{Green - NIR}{Green + NIR}.$$

As water bodies strongly absorb light in visible to infrared electromagnetic spectrum, NDWI uses green and near infrared bands to highlight water bodies. The index was proposed by McFeeters, 1996: water bodies tend to have positive values, while land features such as vegetation and soil typically have lower or negative values. In the context of this study, NDWI was utilized to enhance the detection of flooded areas within the region of interest. By applying NDWI to pre- and post-flood Sentinel-2 images, it

is possible to accurately see the changes in water coverage, highlighting the areas most affected by the flood. This index is especially useful in cases where the presence of water might not be immediately visible in true-color imagery or where water bodies blend with the surrounding land due to similar reflectance characteristics. Through this visualization it is easier to quantify the extent of flooding and assess the damage, as we can see in figure 5 and 6.



Figure 5. Region of interest before the flood: NDWI index.

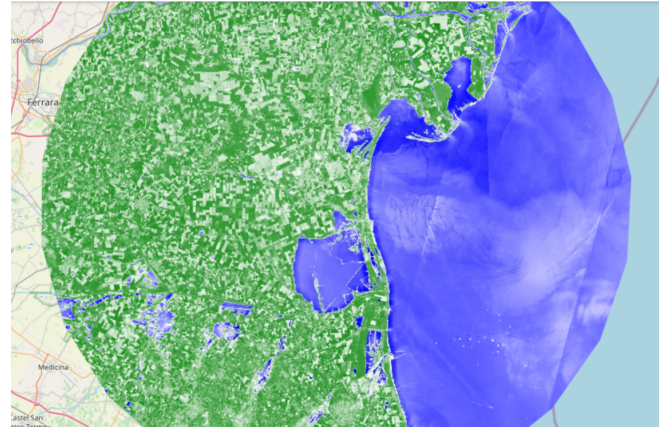


Figure 6. Region of interest after the flood: NDWI index.

3. Change detection techniques

Change detection analysis is a particular procedure that aims to identify occurred changes within an area under investigation. This procedure requires algorithms able to analyze multitemporal acquisitions and extract meaningful information related to the occurred changes. Change detection analysis is one of the main research subjects in remote sensing and represents an important task in practical applications.

To assess the impact of the flood, I focused the study of the change detection analysis on a smaller area that was most affected by the flooding (with coordinates latitude

44.496379, longitude 11.880427, and a buffer of radius of 20 km)². By focusing on this smaller area I could perform a more detailed examination of the changes in land cover and water bodies.

3.1. Histogram comparison

I started by comparing the histograms of the NDWI for the pre- and post-flood images. The NDWI is sensitive to water bodies, making it an ideal index for detecting changes in water coverage.

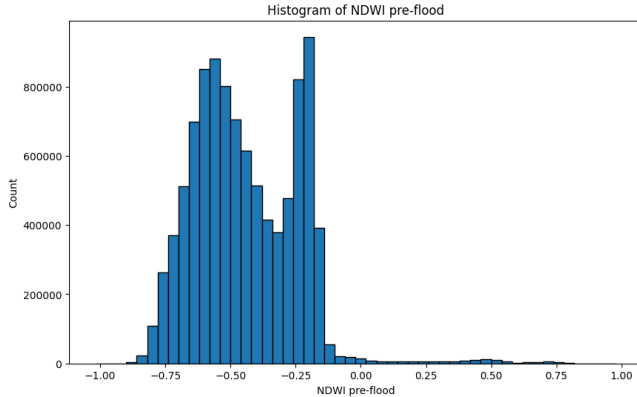


Figure 7. Histogram of NDWI pre-flood.

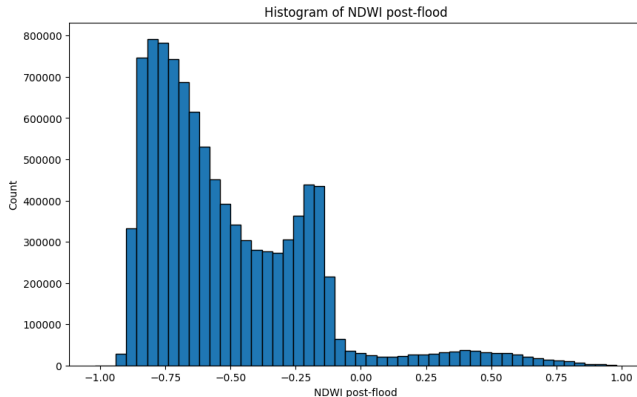


Figure 8. Histogram of NDWI post-flood.

The comparison of these histograms (figures 7 and 8) revealed a clear shift in the distribution of NDWI values, with the post-flood histogram showing an increase in the number of pixels with higher NDWI values, indicating more areas inundated with water. On the contrary, there is a decrease in the number of pixels with lower NDWI values in the post-flood histogram, suggesting a reduction in dry land areas. This comparison visually confirms the extent of the flooding and provides a quantitative measure of the changes in water distribution.

2. The mentioned area can be envisioned in the Appendix section, figure 19

3.2. Ratio

Furthermore, I calculated the ratio between the spectral values of the post-flood and pre-flood images for the NDWI index. In the ratio image, figure 9, pixels that have under-

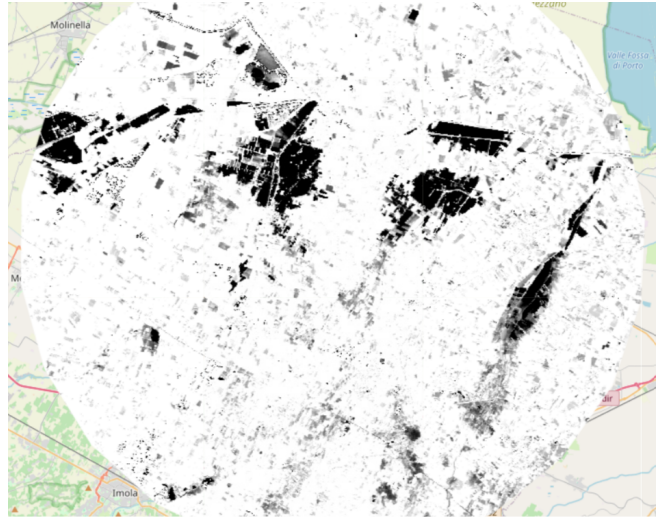


Figure 9. Ratio of NDWI index post- and pre-flood.

gone substantial changes appear darker, while those with minimal or no changes appear brighter.

The image clearly shows several dark spots, corresponding to areas that were likely inundated by floodwaters. These dark spots align with the most severely affected regions as can be compared with figure 19 in the Appendix section. However, it is important to note that the NDWI ratio can have multiple interpretations depending on the specific values corresponding to before and after the flood event. This is because NDWI index ranges between [-1, +1], where water bodies tend to have positive values and land features lower or negative. For example, a ratio greater than 1 could indicate an increase in water presence if both pre-flood and post-flood NDWI values are positive and post-flood index is greater than the pre- one, or an increase in dryness if both values are negative and post-flood index is lower than the pre- one. Conversely, a ratio between 0 and 1 could suggest a decrease in water presence if both values are positive but pre-flood NDWI index is higher than the post, or a reduction in dryness if both values are negative.

Moreover, negative ratios could indicate a transition from a dry state (negative NDWI) to a flooded state (positive NDWI) or vice versa. These cases highlight the need for careful interpretation of the NDWI ratio.

As a consequence, in order to handle this ambiguity I classified the NDWI changes into categories (figure 10):

- Category 1 (blue): "Increase in Water" (Post-NDWI > Pre-NDWI, both positive);
- Category 2 (green): "Decrease in Water" (Post-NDWI < Pre-NDWI, both positive);
- Category 3 (cyan): "From Dry to Water" (Post-NDWI positive, Pre-NDWI negative);

- Category 4 (magenta): "From Water to Dry" (Post-NDWI negative, Pre-NDWI positive);
- Category 5 (red): "Increase in Dryness" (Post-NDWI more negative, both negative);
- Category 6 (yellow): "Decrease in Dryness" (Post-NDWI less negative, both negative).

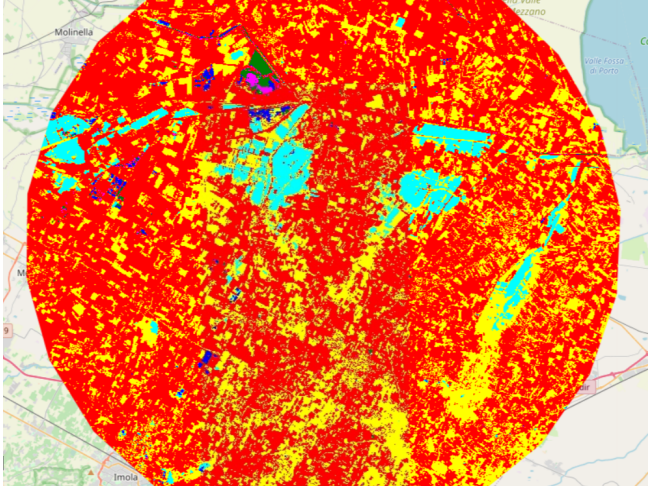


Figure 10. Change categories highlighted through NDWI analysis.

To quantify the amount of change for each category separately I decided to calculate their area:

- Category 1: 6.97 square kilometers;
- Category 2: 5.92 square kilometers;
- Category 3: 56.65 square kilometers;
- Category 4: 3.04 square kilometers;
- Category 5: 798.84 square kilometers;
- Category 6: 372.70 square kilometers.

3.3. Difference

By calculating the difference in NDWI values between pre- and post-flood images, it is possible to effectively highlight areas where significant changes in water coverage occurred. Figure 11 represents the result of the difference between pre- and post-flood: a sharp distinction between water and terrain can be seen, representing a powerful mean in this context. Overall, the NDWI difference technique provides a clear and quantifiable method for assessing the impact of the flood, making it a valuable tool in disaster management and post-event analysis. This is why this result will be exploited further on in this report.

3.4. Change Vector Analysis

Another powerful technique to detect and assess the changes with remote sensing imaging is Change Vector Analysis (CVA). CVA represents one of the most widely used techniques to solve the change detection task because of its simple mathematical definition. CVA usually provides

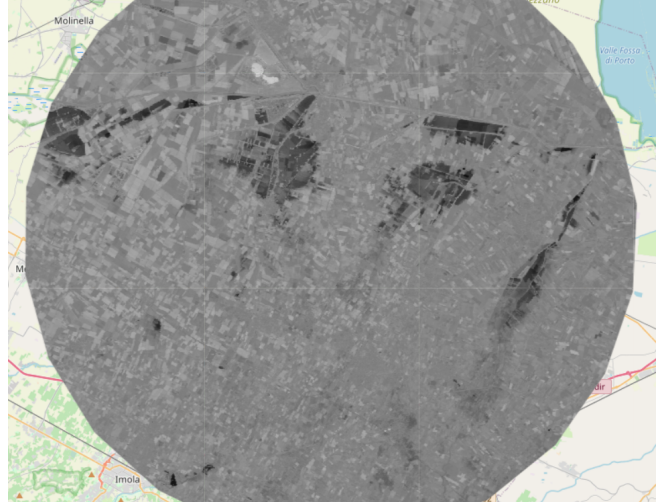


Figure 11. Difference of NDWI index pre- and post-flood.

two outputs: magnitude and phase. The magnitude provides a measure of how much it changed, the phase refers to the angle of change. The calculation of the change magnitude (CM) and the phase or change direction (θ) is presented as follows:

$$CM = \sqrt{\sum_{i=1,j=1}^{i=N,j=B} (D_{i,j}^{c,r} - D_{j,i}^{c,r})^2}$$

$$\theta = \arccos \frac{1}{\sqrt{B}} \left(\sum_{i=1,j=1}^{i=N,j=B} D_{i,j}^{c,r} \right) / \left(\sqrt{\sum_{i=1,j=1}^{i=N,j=B} (D_{i,j}^{c,r} - D_{j,i}^{c,r})^2} \right)$$

N and B denote the total number of images and spectral bands, respectively. D_{ij} is the pixel values in band j for date i at a position (c, r) located by c -column and r -row. The magnitude is essentially the Euclidean distance between the corresponding spectral values in two images (pre and post-event). The direction is measured using the cosine of the angle between the change vector and a reference vector. In order to apply CVA I started with selecting the relevant bands, therefore choosing spectral bands that are sensitive to the changes I wanted to detect. In my case, since I was interested in water changes, I chose B8 and B11, which are particularly sensitive to water content and vegetation changes, making them ideal for flood detection. At this point I proceeded in calculating Change Vectors by computing the difference between the pixel values in the corresponding bands of the images. This results in a change vector for each pixel. Next by determining the length of the change vector for each pixel I found the magnitude of change. At last, in order to find the direction of change, I calculated the angle of the change vector. In this case, since I selected only two bands, the angle is simply the arctangent of the ratio of changes.

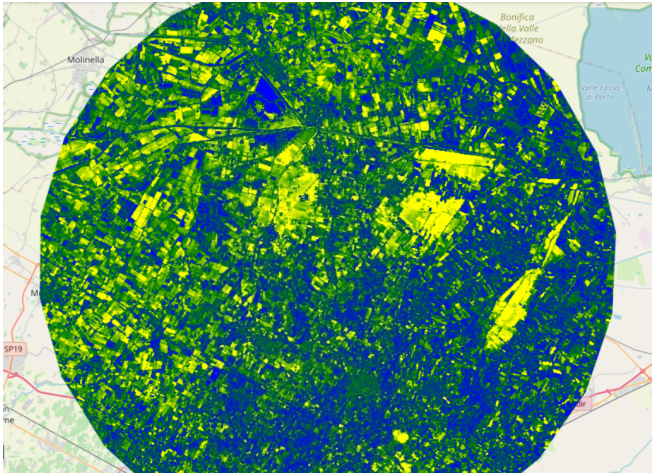


Figure 12. Magnitude of change.

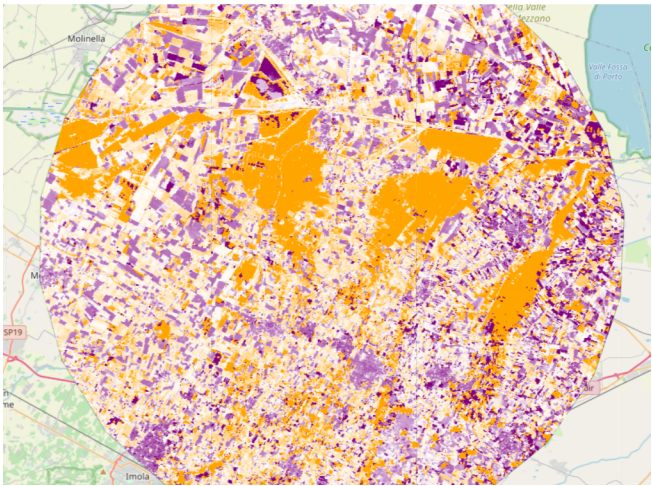


Figure 13. Direction of change.

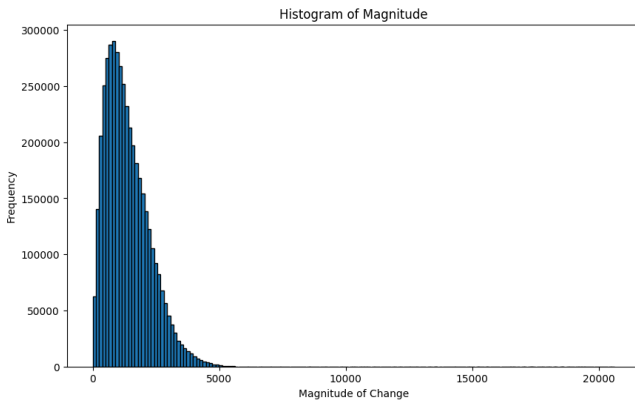


Figure 14. Histogram of the magnitude of change.

To visualize the distribution of magnitude values, a histogram was generated (figure 14). This information is valuable for setting an appropriate threshold for visualizing

the data. The threshold value that I chose is 3000 and acts as a cutoff point, highlighting pixels with changes exceeding that value. Higher magnitude values signify more substantial alterations in the observed features. By visualizing the magnitude with a color gradient ranging from blue to yellow, areas experiencing minimal change appear in blue hues, while regions with the most significant transformations are depicted in yellow.

The direction angle reflects the type of change, such as an increase in vegetation or in water content. To visualize the direction, a color palette ranging from orange to purple was employed, with white representing no significant directional change.

4. Machine Learning

Machine learning offers several significant advantages in the context of remote sensing and change detection, particularly in the analysis of natural disasters like floods. By automating the analysis of large datasets, machine learning algorithms can efficiently process vast amounts of satellite imagery. For this reason, they were added in my study to further explore and understand the changes in the region of interest. Specifically, unsupervised learning methods, such as clustering, were utilized to identify patterns and group pixels in the satellite imagery based on their spectral characteristics. Clustering allows for the segmentation of the landscape into distinct regions, which can be useful for detecting areas affected by the flood without the need for pre-labeled data.

On the contrary, supervised learning techniques were not applied in this study. The first reason for this was the lack of a suitable training dataset. A comprehensive dataset that includes labeled classes specific to flood-affected areas, particularly in the form of satellite imagery, was not available. Supervised learning requires such a dataset to train the model effectively, and since adequate labeled data was absent, it was impractical to employ it in my study. As a consequence, the focus was on unsupervised techniques, which do not require labeled data but can still provide valuable insights into the flood's impact on the landscape. By applying clustering to the difference between pre- and post-flood NDWI index, the algorithm can automatically identify areas where the most substantial changes occurred, which are likely to correspond to flood-affected regions.

The *ee.Clusterer* package handles unsupervised classification (or clustering) in Earth Engine. I opted for k-Means and Learning Vector Quantization (LVQ) algorithms. K-means is one of the most widely used clustering algorithms. The algorithm starts by initializing K centroids randomly. It then iteratively assigns each data point to the nearest centroid and recalculates the centroids based on the current cluster memberships. This process continues until the centroids no longer change significantly, indicating that the clusters are stable.

The objective of Learning Vector Quantization (LVQ) is to organize the data into clusters. In both k-means clustering and learning vector quantization the individual clusters are

represented by a center (or a reference vector). This center is to be positioned in such a way that it lies roughly in the middle of the data point cloud that constitutes the cluster. The two methods mainly differ in how the cluster centers or the reference vectors are adapted. While in k-means clustering the two steps of assigning the data points to the clusters and recomputing the cluster centers as the center of gravity of the assigned data points are alternately executed, learning vector quantization processes the data points one by one and adapts only one reference vector per data point. The procedure is known as competitive learning: the training patterns are traversed one by one. For each training pattern a “competition” is carried out, which is won by the output neuron that yields the highest activation for this training pattern. Only this “winner neuron” is adapted, namely in such a way that its reference vector is moved closer to the training pattern. The result is that the winning neuron is more likely to win the competition the next time a similar vector is presented, and less likely to win when a very different input vector is presented. During training, each neuron in the layer closest to a group of input vectors adjusts its weight vector toward those input vectors. Eventually if there are enough neurons, every cluster of similar input vectors has a neuron that outputs 1 when a vector in the cluster is presented, while outputting a 0 at all other times. As already stated, in order to analyze the impact of the flood, k-means clustering was employed on the difference between the pre- and post-flood NDWI index to automatically segment the region of interest into distinct clusters. By following this approach, areas that have undergone significant changes due to the flood should be found. The training dataset was created by randomly sampling 8,000 pixels from the difference image within the ROI at a spatial resolution of 10 meters. This sample will be the input data for the clustering algorithm. Then, the k-means clustering algorithm is applied with the number of clusters as input (in this case, two) and k-means++ as initialization method for the cluster centers. In fact, k-means++ is more powerful with respect to classic k-means: the random initialization of the initial k-means centroids can lead to poor clustering results if they are not well chosen; the algorithm might indeed converge to a local minimum rather than the global minimum. Moreover, with poor initial centroids, k-means algorithm may require a large number of iterations to converge. On the contrary, k-means++ is a robust way of selecting the K initial cluster centers: it selects an initial point at random to be the first centroid, then, for $K - 1$ steps, for each of the N points, x_i , $1 \leq i \leq N$, find the minimum squared distance to the currently selected centroids, C_1, \dots, C_K , $1 \leq j \leq K$, i.e., $\min_j d^2(C_j, x_i)$. At this point it randomly selects a new centroid by choosing a point with probability proportional to $\frac{\min_j d^2(C_j, x_i)}{\sum_i \min_j d^2(C_j, x_i)}$.

The algorithm was trained using the sampled dataset just described. The choice of two clusters was based on the assumption that the ROI could be divided into two main classes: flooded and non-flooded areas. Finally, the trained k-means clusterer was applied to the entire difference image

(restricted to the ROI). This process assigned each pixel in the ROI to one of the two clusters, effectively segmenting the landscape into regions that are similar in terms of the changes detected between the pre- and post-flood images. A similar approach was also taken with Learning Vector Quantization. The idea is to further refine the identification of flood-affected areas and to see if any new aspects emerge that were not previously identified. As before the training dataset was created by sampling the difference pixels within the ROI. This dataset would be the input for the LVQ algorithm. An LVQ clusterer was then instantiated with the number of clusters, two, as input and trained using the sampled dataset. The trained LVQ model was then applied to the difference image, resulting in a segmented map of the ROI. The intention of this analysis is to benefit from multiple perspectives on how the flood affected the region.

5. Results and validation

K-means clustering applied to the difference in NDWI index effectively identified significant changes in water coverage across the area of interest, with the blue regions in figure 15 representing areas affected by the flood. These clusters are dispersed across the image, once again highlighting the extent of the damages. As it regards LVQ

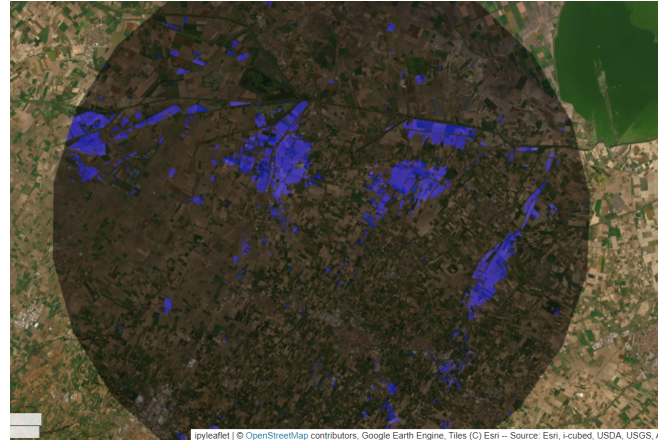


Figure 15. K-means clustering result.

clusters, a similar segmentation map can be observed in figure 16: the more extended principal flooded areas are found, though some minor zones that were detected as flood water by k-means algorithm are not recognised.

In order to inspect the differences between the two clustering results, I applied the difference of the two results, leading to figure 17.

As already noticed, it is now clearer that k-means found wider areas and more isolated flooded spots. To have another proof of the differentiation between the two results, I measured the area of the flooded regions for both the k-means and LVQ mask, leading to approximately 99 km^2 and 53 km^2 respectively.

To ensure the robustness and accuracy of my findings, it



Figure 16. Learning Vector Quantization clustering result.



Figure 17. Difference between k-means and LVQ clustering results.

was crucial to validate the results through a comparison with authoritative reference data. In this way I would have been able to compute accuracy metrics, true positives, false positives, true negatives, false negatives and, as a consequence, to understand and eventually improve my study. However, I encountered some challenges in searching a comprehensive and authoritative reference map in a suitable format that would allow me for the validation of my methods. Consequently, the validation of my results had to rely on a qualitative approach. The validation of my flood mapping results was conducted by visually comparing the flood maps (figure 18) available from authoritative sources [9]. Although informative, it did not provide the level of detail or accuracy required for a rigorous validation process. Nevertheless, it visually corresponds with my findings, especially k-means++ result, confirming the robustness of the methodology.

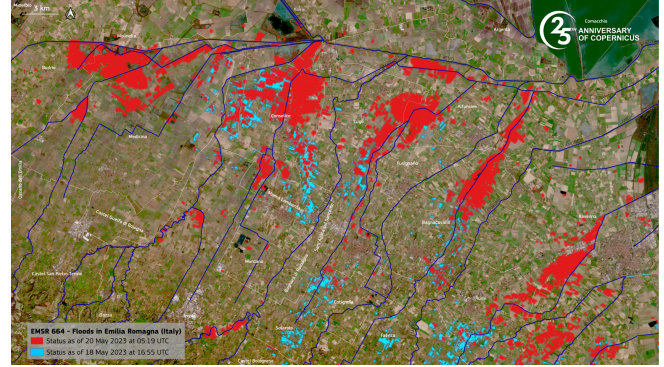


Figure 18. True flooded map.

6. Conclusions

In this report, I utilized Sentinel-2 imagery to analyze and map the extent of the Emilia-Romagna flood that occurred in May 2023. Through the exploitation of band combination, ratio and difference calculation between pre- and post-flood event, histogram comparison, change vector analysis, and unsupervised clustering algorithms, I have achieved a detailed segmentation of the flooded areas. The validation conducted by visually inspecting my results against authoritative flood maps confirms the accuracy and reliability of my findings, demonstrating the efficiency of these remote sensing techniques in flood assessment.

The study in this report not only highlights the capabilities of Sentinel-2 imagery for flood monitoring but also sets a foundation for further researches. To enhance the understanding of the flood dynamics and improve predictive capabilities, future researches could incorporate time series analysis. In fact, in time series analysis, data points are recorded at consistent intervals over a set period of time rather than just recording the data points intermittently or randomly. In this way it can be shown how variables change over time or, in other words, how the data adjusts over the course of time until the final results. Furthermore it's a powerful tool for making sense of the past and using that understanding to predict the future, with, for instance, the support of Long Short-Term Memory (LSTM), a popular deep learning model that has proven to be effective in capturing temporal dependencies and making accurate predictions. In the context of my studies, this approach would enable the examination of flood progression over time, offering deeper insights into the temporal aspects of flood events and their impacts and could be crucial in identifying potential risks, guide decisions. Overall, the insights gained from my analysis contribute in giving valuable information for flood management and disaster response, and a further investigation with the proposed time series analysis could provide a more comprehensive view of flood phenomena.

Another suggestion for future work in the context of this project could be the benefit from the availability of high-resolution, authoritative flood maps that can facilitate more precise accuracy assessments and contribute to more reliable

conclusions.

To conclude, the visual agreement between my results and the authoritative maps provides a solid foundation for further analyses and potential applications in flood management and response planning.

References

- [1] Rudolf Kruse and Sanaz Mostaghim and Christian Borgelt and Christian Braune and Matthias Steinbrecher, *Computational Intelligence - A Methodological Introduction*, 3rd edition, Springer, 2022
- [2] S. D. Sapkal, S. N. Kakarwal and P. S. Revankar, *Analysis of Classification by Supervised and Unsupervised Learning*, International Conference on Computational Intelligence and Multimedia Applications (ICCIMA 2007), 2007
- [3] ZhiYong, Lv and Wang, FengJun and Xie, LinFu and Sun, WeiWei and Falco, Nicola and Benediktsson, Jón Atli and You, ZhenZhen, *Diagnostic Analysis on Change Vector Analysis Methods for LCCD Using Remote Sensing Images*, IEEE Journal of Selected Topics in Applied Earth Observations and Remote Sensing, 2021
- [4] *Satellites map aftermath of Emilia-Romagna floods*, https://www.esa.int/Applications/Observing_the_Earth/Satellites_map_aftermath_of_Emilia-Romagna_floods
- [5] *S2 Mission. Overview of Sentinel-2 Mission*, <https://sentiwiki.copernicus.eu/web/s2-mission>
- [6] *FRAMEWORK SERVICE CONTRACT FOR COPERNICUS EMERGENCY MANAGEMENT SERVICE RISK & RECOVERY MAPPING, TECHNICAL REPORT, EMSN154: Flood in Emilia-Romagna, Italy*
- [7] *Detecting Changes in Sentinel-1 Imagery*, <https://developers.google.com/earth-engine/tutorials/community/detecting-changes-in-sentinel-1-imagery-pt-1>
- [8] *Unsupervised Classification (clustering)*, <https://developers.google.com/earth-engine/guides/clustering>
- [9] *Historic floods hit Emilia-Romagna, Italy*, <https://www.copernicus.eu/en/media/image-day-gallery/historic-floods-hit-emilia-romagna-italy>
- [10] *Normalized Difference Water Index, NDWI*, <https://custom-scripts.sentinel-hub.com/custom-scripts/sentinel-3/ndwi/>
- [11] Federico De Guio and Matteo Fossati, *Lectures' slides of Signal and imaging acquisition and modelling in environment*, Università degli Studi di Milano Bicocca, 2024
- [12] Fabio Stella, *Lectures' slides of Unsupervised Learning*, Università degli Studi di Milano Bicocca, 2024

7. Appendix

TABLE 1. SENTINEL-2 BANDS CHARACTERISTICS

Sentinel-2 Bands	Central Wavelength (μm)	Resolution (m)
Band 1 - Coastal aerosol	0.443	60
Band 2 - Blue	0.490	10
Band 3 - Green	0.560	10
Band 4 - Red	0.665	10
Band 5 - Vegetation Red Edge	0.705	20
Band 6 - Vegetation Red Edge	0.740	20
Band 7 - Vegetation Red Edge	0.783	20
Band 8 - NIR	0.842	10
Band 8A - Vegetation Red Edge	0.865	20
Band 9 - Water vapour	0.945	60
Band 10 - SWIR - Cirrus	1.375	60
Band 11 - SWIR	1.610	20
Band 12 - SWIR	2.190	20

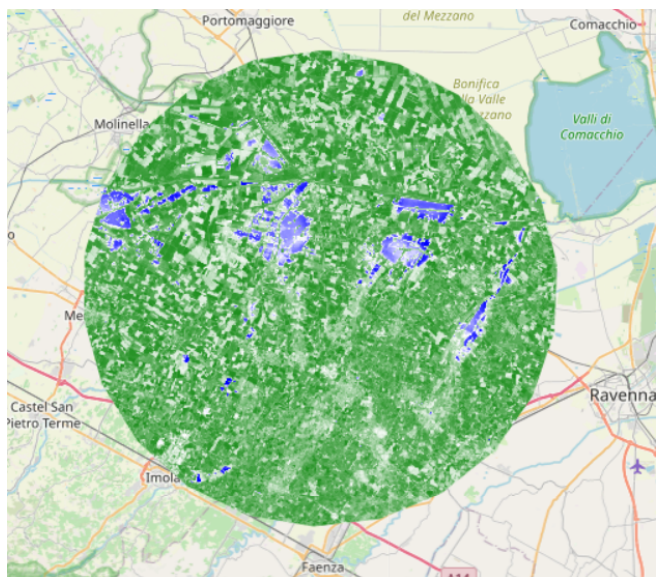


Figure 19. Flooded region: NDWI index.